Micromechanical model for elasticity of the cell cytoskeleton

Sitikantha Roy and H. Jerry Qi*
Department of Mechanical Engineering, University of Colorado, Boulder, Colorado 80309, USA
(Received 31 March 2008; revised manuscript received 21 May 2008; published 18 June 2008)

Semiflexible polymer networks, such as cell cytoskeleton, differ significantly from their flexible counterparts in their deformation energy storage mechanism. As a result, the network elasticity is governed by both enthalpic and entropic variations. In addition, the enthalpic effect shows two distinct regimes of energy storage mechanism, the affine and nonaffine regimes. In the past, computation-based modeling on random networks, such as the Mikado model, was used to demonstrate the physical mechanism of mechanical deformation of semiflexible networks. These models are computationally intensive and hence are difficult to apply to studying whole cells. In this paper, we develop a micromechanical model to predict the average macroscopic elastic properties of a random, semiflexible, biopolymer network. The model employs a unit cell consisting of four semiflexible chains and four equivalent axial-bending springs. The proposed unit-cell-based micromechanical model represents a statistically average realization of the actual network and gives the average mechanical properties, such as the shear modulus. Comparisons between the model predictions and Mikado model results confirm that this micromechanical model captures the essential deformation physics revealed from previous studies on the actual network and is capable of predicting the transition between nonaffine and affine deformations. This model can be used to develop efficient continuum constitutive models of the cytoskeleton in the future.

DOI: 10.1103/PhysRevE.77.061916 PACS number(s): 87.16.Ln, 87.16.Ka, 87.15.La, 87.17.Rt

I. INTRODUCTION

Cells are the basic functional units of life. To perform their various life-sustaining activities, cells undergo and control a plethora of intra- and extracellular events, many of which involve mechanical phenomena, such as mechanotransduction between the cell and its external environment [1]. In most eukaryotic cells, the mechanical and dynamical properties are governed by a network of biopolymers that collectively form what is known as the *cytoskeleton*, a moderately flexible and dynamic network of protein fibers of varying lengths and mechanical properties combined with a group of associated regulatory proteins [2] (Fig. 1). The major constituent biopolymers of cytoskeleton are actin filaments (AFs), intermediate filaments (IFs), and microtubules (MTs). The cytoskeleton manages the arrangements of these constituent biopolymers to bring about systematic changes in the macroscopic mechanical properties during the cell's mechanical interaction with the extracellular environment, commonly called the extracellular matrix (ECM). Cell motility, division, and adhesion are some of the well-known activities at the macroscopic level where the mechanical properties of the cytoskeleton play an important role. Studies on the single-molecular level [3–6] have established that the constituent biopolymers of the cytoskeleton behave like semiflexible polymers and contribute in a unique manner to the macroscopic network elasticity of the cell cytoskeleton.

In a flexible polymer network such as a rubber, the persistence length of a polymer chain is much smaller than the distance between two cross-linking sites [7]. Therefore, individual polymer chains can undergo continuous thermal fluctuations, which give rise to entropic behaviors. The elasticity is thus contributed by entropic variations and the strain energy is mainly stored entropically due to the reduction of the number of accessible chain conformations between the cross links [8]. In a network consisting of semiflexible polymer chains, the persistence length l_p of the individual chains is much longer than the average distance between the two cross-link sites, l_c, and comparable to the contour length of individual polymer chains, L. As a consequence, a cross-linked network made of semiflexible polymer differs significantly from a flexible polymer network in its elastic energy storage mechanism and overall macroscopic manifestation of elastic behavior. In a semiflexible polymer network, deformation energy is contributed by both entropic as well as enthalpic variation. In addition the latter is stored in extensional, bending, or coupled modes in the network.

At the microscopic level, where the individual chains are deformed to accommodate the macroscopic deformation, only one length scale l_c dictates the overall process in a flexible polymer network. The identity of an individual flexible chain is lost on a length scale beyond the cross-linking distance (neglecting the dangling end effect and the excluded

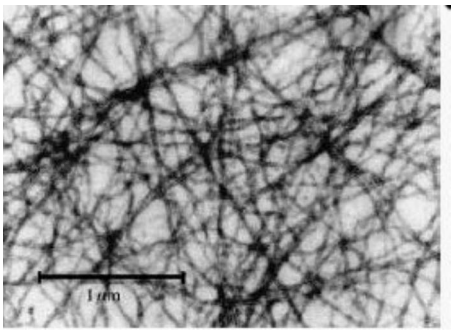

FIG. 1. Electron microscope image of semidilute solution of cytoskeleton [32].

*Corresponding author. qih@colorado.edu

volume interaction) [9]. On the contrary, a semiflexible polymer chain can retain its identity beyond a cross-link point, because the two segments in the chain can still be correlated over distances much longer than l_c [9]. The cross-linking density, defined as the number of cross links over a polymer chain and calculated as L/l_c-1, has a significant effect in determining the overall elasticity of a semiflexible network [9–11]. Another significant difference in flexible network elasticity is that deformation is assumed to be spatially uniform down to the smallest microscopic length scale in the material. The affine deformation assumption is a great simplification that allows the construction of theoretical models relating the macroscopic elastic constants of a flexible polymer network to the microscopic properties of its constituent polymers [12]. For modeling semiflexible networks, however, recent theoretical studies have revealed that application of the affine approximation is not adequate; rather a crossover between the spatially uniform affine deformation and the spatially heterogeneous nonaffine deformation takes place depending on the length scale and the degree of cross linking in the network [9–11,13,14]. At the macroscopic scale, which is on the order of the sample size, all deformations self-average to maintain an affine uniformity, but this self-averaging does not hold in all successively smaller mesoscopic and microscopic length scales. Identifying this elusive length scale is an important step toward predicting the correct homogenized elastic properties of a semiflexible network [15]. Also, it has recently been found in the literature [9,13,16] that for a given set of elastic parameters (bending stiffness and axial stiffness) of the individual constituents of a semiflexible network, the transition between nonaffine and affine deformations is characterized by a transition between the deformation dominated by the bending mode (nonaffine) and the one dominated by the stretching mode (affine). At low cross-linking density, bending is the favorable deformation mode since it requires lower energy; the deformation of the network is therefore nonaffine. As the cross-linking density increases, the cross-linking sites become closer to each other; as a consequence the attachments of polymer chains impose strong resistance to the transverse deflection of a chain and hence impede the bending deformation; at high cross-linking density, the stretching deformation dominates and the network deformation becomes affine [9,13].

Recently, the growing interest in cytoskeleton mechanics has necessitated the development of efficient models that can capture the essential physical mechanism of cytoskeleton deformation as discussed above. Previous studies view a cytoskeleton as a single-phase, random percolation, network of discrete filamentous elements [1,11,13,17], such as the Mikado model (Fig. 2) considered by Head *et al.* [9,13] and Wilhelm and Frey [11], where they carried out finite-element analysis of a unit cell derived from the actual network for different realizations (different distributions of cross links and relative orientations) to find the dependence of the average macroscopic shear and extensional modulus of the whole network on the varying geometrical and material parameters. Significant physical insight can be gained from such a model. For example, they found that for semiflexible network, the nonaffine to affine transition is represented by vanishing bending energy contribution to the overall deformation. However, such a modeling methodology is computationally expensive, even with the unit cell model used in their studies. Such a modeling methodology, if not impossible, will be even more expensive at the whole cell level. One strategy to improve the efficiency is to develop a continuum level constitutive model where the cytoskeleton will be viewed as a continuum medium but has the same strain energy as the actual cytoskeleton in response to deformation. Such a development will need an analytical description of the strain energy associated with general deformations in the cytoskeleton, upon which the stress-strain relationship can be readily obtained [18]. In this paper, we propose a micromechanical model for the cross-linked actin filamentous network through a unit cell consisting of four semiflexible chains, where the internal balance of bending and stretching will be manifested in its homogenized constitutive results at the macroscopic scale. This micromechanical approach has been used in the past to develop constitutive models for different materials, including polymer networks such as rubbers [19]. In this paper, we first consider the enthalpic contribution to the macroscopic elasticity and the network is assumed to be at $T=0$ K. Inclusion of the entropic contribution is discussed after the presentation of the model. The network is also assumed to span a sufficiently large domain compared to the individual chain length so that we can neglect the finite-size effects [14].

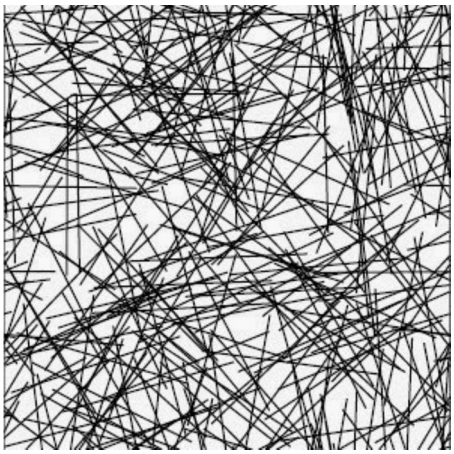

FIG. 2. 2D random network of fibers, $L/l_c=29.09$, Mikado model [13].

II. MODEL DESCRIPTION

In the following, we present a model based on a unit cell consisting of four semiflexible polymer chains. It is important to note that the present unit cell arrangement provides a framework that one can use to develop a representative cell with different numbers of fibers, for example, a three-fiber triangular unit cell. However, a triangular unit cell would incorporate anisotropy with respect to stretch. Therefore, unless the network has an inherent topological pattern that is close to a triangular network (such as a spectrin network [20,21]) and exhibits inherent anisotropy, a four-fiber unit will present a reasonable approximation of the real material.

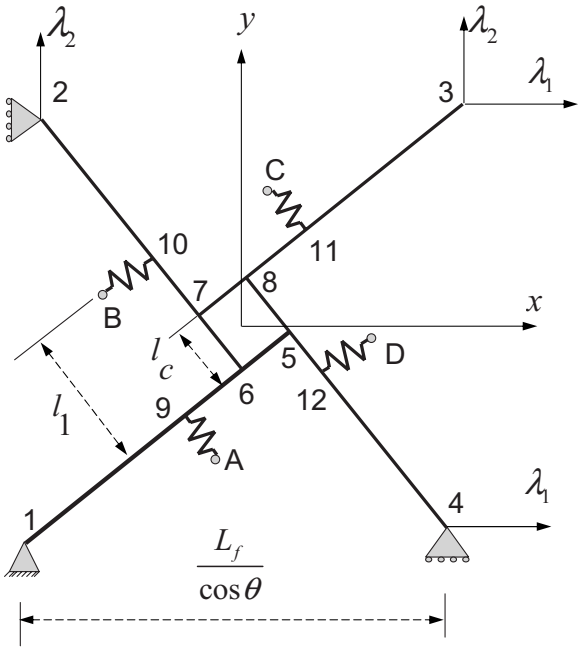

FIG. 3. Unit cell idealization of a cytoskeleton.

Certainly, one may consider a unit cell with more chains, such as an eight-fiber unit; as long as they are properly arranged, one may obtain a better approximation. However, previous developments of models for rubber elasticity showed that, although more fibers in the unit can improve the model prediction, the amount of improvement is not significant as compared to the additional complicated mathematical work involved [19].

A. A unit cell: Representative of cytoskeleton

In the micromechanical model, the unit cell is made of four semiflexible polymer chains connected with each other as shown in Fig. 3. The global coordinate axes (x,y) are placed at the center of the unit cell. The chains $L_{1\text{-}9\text{-}6\text{-}5}$, $L_{2\text{-}10\text{-}7\text{-}6}$, $L_{3\text{-}11\text{-}8\text{-}7}$, $L_{4\text{-}12\text{-}5\text{-}8}$ represent four semiflexible chains of length L_f each and will be termed the four *main chains* from here on. The main chains connect with each other to form an internal square (6-7-8-5) with each side length l_c. Here l_c represents the average distance between two consecutive cross links in the network. The joints are assumed to be flexible hinges to simulate the mechanical linkages at the cross links in the actual network. As revealed in previous studies, changing the cross-link connections from the hinge to the weld type does not affect the overall model predictions significantly [13,22]. The main chains have an angle 90° with each other at a joint. In addition, the main chains are also attached with four equivalent springs at nodes 9, 10, 11, and 12 at a distance l_1 from the nodes 5, 6, 7, and 8, respectively (shown in Fig. 3). The springs are used to simulate constraints applied to these four main chains from the other chain attachments due to axial stretching and bending in the actual network. It is also assumed that the base nodes A, B, C, and D of the four equivalent springs are embedded in space and move affinely with the applied stretches. λ_1 and λ_2

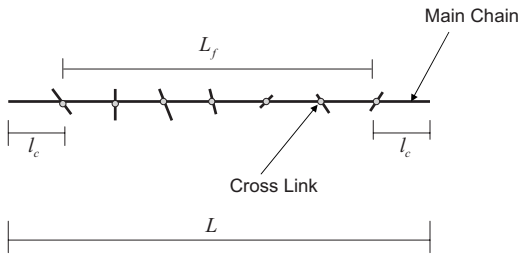

FIG. 4. Actual and effective lengths of the main chains.

are the applied principal stretches on the unit cell. The boundary conditions are imposed as shown in Fig. 3, in order to eliminate the rigid body motions of the system. The material properties of the individual chains are given by two parameters: the bending stiffness κ and the axial stiffness μ. Following Head *et al.* [9,13], we define a nondimensional material parameter as

$$\bar{l}_b = l_b/L = \sqrt{\frac{\kappa}{\mu}}\frac{1}{L}. \tag{1}$$

Any mechanical property of the network can be expressed as a function of two nondimensional parameters L/l_c and l_b/L. For a given geometric parameter L/l_c, the average number of cross links over a semiflexible chain in the network is $L/l_c - 1$. We define the effective length of each chain as (neglecting the dangling ends at each end; see Fig. 4)

$$L_f = L - 2l_c. \tag{2}$$

In Fig. 3, the equivalent spring represents the overall constraints (due to bending and axial loading of chains attached to the main chain) from other chain attachments in the actual network and l_1 is the distance between the base node of the equivalent spring and the attachment point to the main chain (see Fig. 5). Based on this concept, l_1 is defined to be the average distance of $(L_f/l_c+1)-2$ cross links attached to the main chain between distances l_c and L_f, measured from one

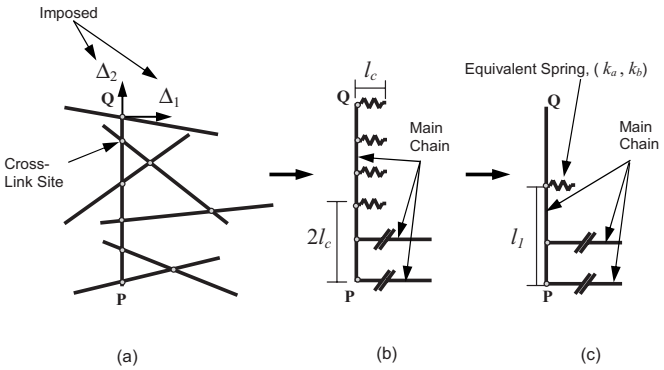

FIG. 5. (a) Cross-link arrangements in the actual network. (b) Average attachment of the cross-linked elements on the main chain. The last two attachments are attached to the main chain in the unit cell; all other attachments are replaced by axial-bending springs. (c) Equivalent spring [the equivalent of all the springs in (b)] and its attachment to the main chain.

end of the chain as shown in Fig. 5(c). The expression of the distance l_1 is given by

$$l_1 = \frac{2l_c + 3l_c + \cdots + (L_f/l_c - 1)l_c}{(L_f/l_c - 1)} = \frac{1}{2}(L_f/l_c + 2)l_c. \quad (3)$$

In Figs. 5(b) and 5(c), $L_f/l_c - 1$ polymer chains are attached to a main chain within the distance l_c. The overall contribution of these chains is represented by an equivalent spring of length l_c and axial stiffness (k_a) and bending stiffness (k_b). To estimate the axial and bending spring stiffness, we calculate the energy equivalence corresponding to imposed displacements Δ_1 and Δ_2 at one end relative to the other end of a main chain. The expressions of the spring constants are given by

$$k_a = \frac{2}{3}\frac{\mu}{L_f}\frac{(L_f/l_c)^m(L_f/l_c + 1)(2L_f/l_c + 1) - 1}{(L_f/l_c + 2)^2},$$

$$k_b = \frac{3\kappa}{L_f^3}\frac{(L_f/l_c)^{n+3}}{(L_f/l_c - 1)}, \quad (4)$$

where m and n are two fitting exponents, incorporated as a correction to account for the difference between the estimation from Eq. (4) and the actual network. As discussed later, m and n are determined by comparing the unit cell model prediction and the actual network analyses in the literature and are determined to be $m=1$ and $n=3$. For the present unit cell idealization, these exponents remain constants and are independent of variations of the cross-link density and other material parameters.

B. Strain energy of deformation

We now calculate the strain energy stored in the unit cell due to the applied stretches. The total energy can be given as

$$U = U^a_{\text{ch}} + U^b_{\text{ch}} + U^a_{\text{sp}} + U^b_{\text{sp}}, \quad (5)$$

where the superscripts a and b stand for axial and bending, respectively, and the subscripts "ch" and "sp" denote chains and springs, respectively. The bending energy in terms of the nodal displacements u_i and v_i (u_i is the displacement of a node along the main chain and v_i is the displacement perpendicular to the main chain.) is given as

$$\begin{aligned} U^b_{\text{ch}} &= U^b_{\text{1-9-6-5}} + U^b_{\text{2-10-7-6}} + U^b_{\text{3-11-8-7}} + U^b_{\text{4-12-5-8}} \\ &= \frac{6\kappa}{L_f^3}\frac{(L_f/l_c)^3(L_f/l_c - 1)}{4(L_f/l_c)(l_1/l_c) - (1 + l_1/l_c)^2}(\Delta^2_{\text{1-9-6-5}} + \Delta^2_{\text{2-10-7-6}} \\ &\quad + \Delta^2_{\text{3-11-8-7}} + \Delta^2_{\text{4-12-5-8}}), \end{aligned} \quad (6)$$

where

$$\Delta_{\text{1-9-6-5}} = \left(v_5 - \frac{\alpha}{\alpha - \beta}v_9\right) - \frac{\beta}{\beta - 1}\left(-u_6 - \frac{\alpha - 1}{\alpha - \beta}v_9\right) \quad (7)$$

$$\Delta_{\text{2-10-7-6}} = \left(v_6 - v_2 - \frac{\alpha}{\alpha - \beta}(v_{10} - v_2)\right) - \frac{\beta}{\beta - 1}\left(-u_7 - v_2 - \frac{\alpha - 1}{\alpha - \beta}(v_{10} - v_2)\right)$$

$$\Delta_{\text{3-11-8-7}} = \left(v_7 - v_3 - \frac{\alpha}{\alpha - \beta}(v_{11} - v_3)\right) - \frac{\beta}{\beta - 1}\left(-u_8 - v_3 - \frac{\alpha - 1}{\alpha - \beta}(v_{11} - v_3)\right)$$

$$\Delta_{\text{4-12-5-8}} = \left(v_8 - v_4 - \frac{\alpha}{\alpha - \beta}(v_{12} - v_4)\right) - \frac{\beta}{\beta - 1}\left(-u_5 - v_4 - \frac{\alpha - 1}{\alpha - \beta}(v_{12} - v_4)\right),$$

and $\alpha = L_f/l_c$, $\beta = l_1/l_c$.

The axial energy U^a_{ch} is given as

$$U^a_{\text{ch}} = U^a_{\text{1-9-6-5}} + U^a_{\text{2-10-7-6}} + U^a_{\text{3-11-8-7}} + U^a_{\text{4-12-5-8}}, \quad (8)$$

where

$$U^a_{\text{1-9-6-5}} = \frac{1}{2}\frac{\mu}{L_f}\alpha\left(\frac{u_9^2}{\alpha - \beta} + \frac{(v_6 - u_9)^2}{\beta - 1} + (u_5 - v_6)^2\right) \quad (9)$$

$$U^a_{\text{2-10-7-6}} = \frac{1}{2}\frac{\mu}{L_f}\alpha\left(\frac{(u_{10} - u_2)^2}{\alpha - \beta} + \frac{(v_7 - u_{10})^2}{\beta - 1} + (u_6 - v_7)^2\right)$$

$$U^a_{\text{3-11-8-7}} = \frac{1}{2}\frac{\mu}{L_f}\alpha\left(\frac{(u_{11} - u_3)^2}{\alpha - \beta} + \frac{(v_8 - u_{11})^2}{\beta - 1} + (u_7 - v_8)^2\right)$$

$$U^a_{\text{4-12-5-8}} = \frac{1}{2}\frac{\mu}{L_f}\alpha\left(\frac{(u_{12} - u_4)^2}{\alpha - \beta} + \frac{(v_5 - u_{12})^2}{\beta - 1} + (u_8 - v_5)^2\right).$$

The energy stored in the four equivalent springs is given as

$$U^a_{\text{sp}} = \frac{1}{2}k_a[(v_9 - v_A)^2 + (v_{10} - v_B)^2 + (v_{11} - v_C)^2 + (v_{12} - v_D)^2],$$

$$U^b_{\text{sp}} = \frac{1}{2}k_b[(u_9 - u_A)^2 + (u_{10} - u_B)^2 + (u_{11} - u_C)^2 + (u_{12} - u_D)^2], \quad (10)$$

where (u_A, v_A), (u_B, v_B), (u_C, v_C), and (u_D, v_D) are the corresponding displacements at points A, B, C, and D. With the externally applied stretches and the imposed boundary conditions, we minimize the total potential of the system to solve the nodal displacements. The strain energy of deformation is expressed as a quadratic function of the applied stretches. The energy stored per unit area is then calculated as

$$U^*(\lambda_1^2, \lambda_2^2) = \frac{U}{A_{\text{uc}}}, \quad (11)$$

where U is the total energy stored inside the unit cell. The area of the unit cell is given as (see Fig. 3)

$$A_{\text{uc}} = (L_f/\cos\theta)^2, \quad \tan\theta = 1 - \frac{l_c}{L_f}. \quad (12)$$

C. Elastic modulus calculation

The network is assumed to be statistically isotropic in nature. For any kind of imposed deformation in two dimensions (2D), there exist two principal stretch directions [23]. To calculate the shear modulus, we impose a shear strain of magnitude γ on the unit cell. The principal stretches can be expressed in terms of the applied shear deformation in the small-strain limit as

$$\lambda_1 = 1 + \frac{\gamma}{2}, \quad \lambda_2 = 1 - \frac{\gamma}{2}. \tag{13}$$

The shear modulus is given by

$$G^* = \frac{d^2}{d\gamma^2} U^*(\gamma^2). \tag{14}$$

It is well known that the elastic modulus of a random 2D fibrous network follows a power law behavior near the rigidity percolation threshold [24–28]. The rigidity percolation is the minimum cross-linking density above which the network shows a finite rigidity. For the present case we use the value reported for a 2D rod network by Latva-Kokko *et al.* where $L/l_c|_{\text{crit}} = 5.932$ [29]. The unit cell modulus should give a reasonable estimate of the shear modulus of the actual network near and away from the percolation threshold. For this reason, we incorporate an *ad hoc* type of functional correction given by $C(L/l_c - 5.932)^f$. The actual network modulus is then represented as

$$G = G^* C(L/l_c - 5.932)^f. \tag{15}$$

By making a best fit approach with the actual network analysis [13] (discussed later), we estimate the parameters as $C = 0.035$ and $f = 1.4 \pm 0.2$.

III. RESULTS AND DISCUSSIONS

A. Model parameters

In order to obtain the parameters m and n in Eq. (4), we fit G/G_{affine} vs l_b/L for the case of $L/l_c = 29.09$ in Head *et al.* [13], as shown in Fig. 6(a). Here, G_{affine} is defined as [13]

$$G_{\text{affine}} = \lim_{\kappa \to \infty} G. \tag{16}$$

An approximate expression (see the Appendix) of G_{affine} for moderately large cross-link density, i.e., $\alpha = L_f/l_c \approx L/l_c$, is given by

$$G_{\text{affine}} = 2\mu L \left(\frac{C(\alpha - 5.932)^f}{A_{\text{uc}}} \right) \left(\frac{2\alpha^4 - 9\alpha^3 + 11\alpha^2 + 3\alpha}{(\alpha - 2)^3(1 + 2\alpha)} \right). \tag{17}$$

It is seen that the functional correction in Eq. (15), $C(L/l_c - 5.932)^f$ does not affect the G/G_{affine} value (as it is a ratio) and the exponents m and n represent the fundamental contribution of the unit cell with four springs only. This curve fitting results in $m = 1$ and $n = 3$.

To obtain the parameters in Eq. (15), we fit the data from actual network analysis [13] with various L/l_c and l_b/L $= 0.006$ as shown in Fig. 7(a), and the parameters are estimated as $C = 0.035$ and $f = 1.4 \pm 0.2$.

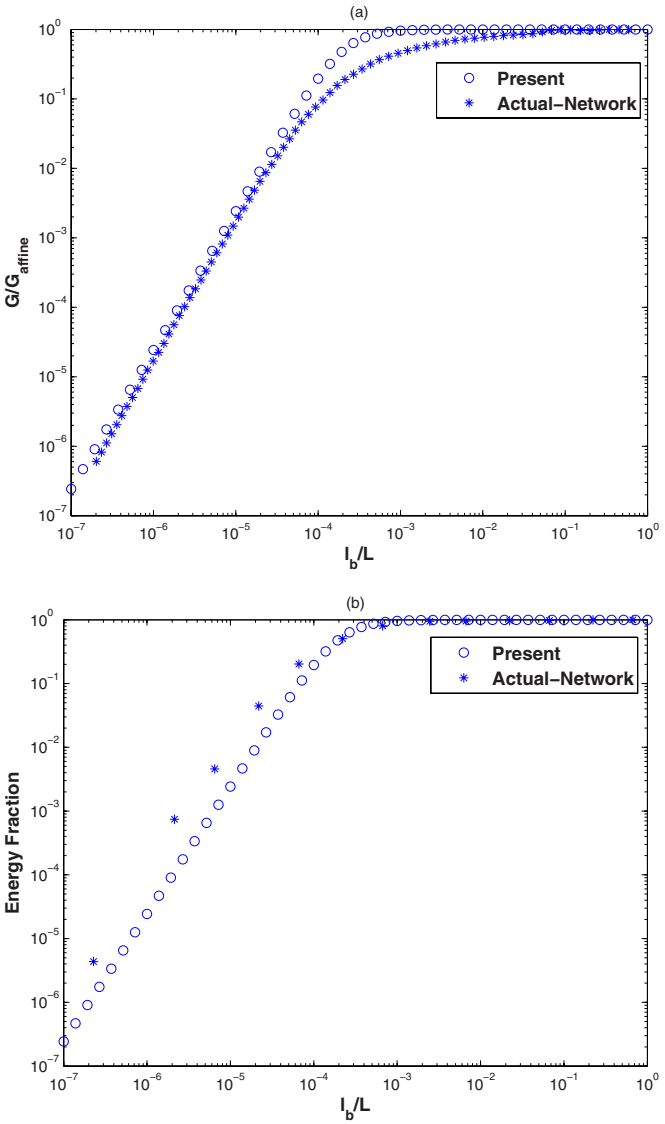

FIG. 6. (Color online) (a) Normalized shear modulus G/G_{affine} vs l_b/L and $L/l_c = 29.09$; (b) axial energy fraction for the same case. The actual network prediction is from the Mikado model [13].

B. Results

We further evaluate the variation of the axial energy contribution. The axial energy fraction is defined as

$$\frac{U_{\text{axial}}}{U} = \frac{U^a_{\text{ch}} + U^a_{\text{sp}}}{U^a_{\text{ch}} + U^a_{\text{sp}} + U^b_{\text{ch}} + U^b_{\text{sp}}}. \tag{18}$$

An approximate expression (see the Appendix) for the axial energy fraction for moderately large cross-link density i.e., $\alpha = L_f/l_c \approx L/l_c$, is given by

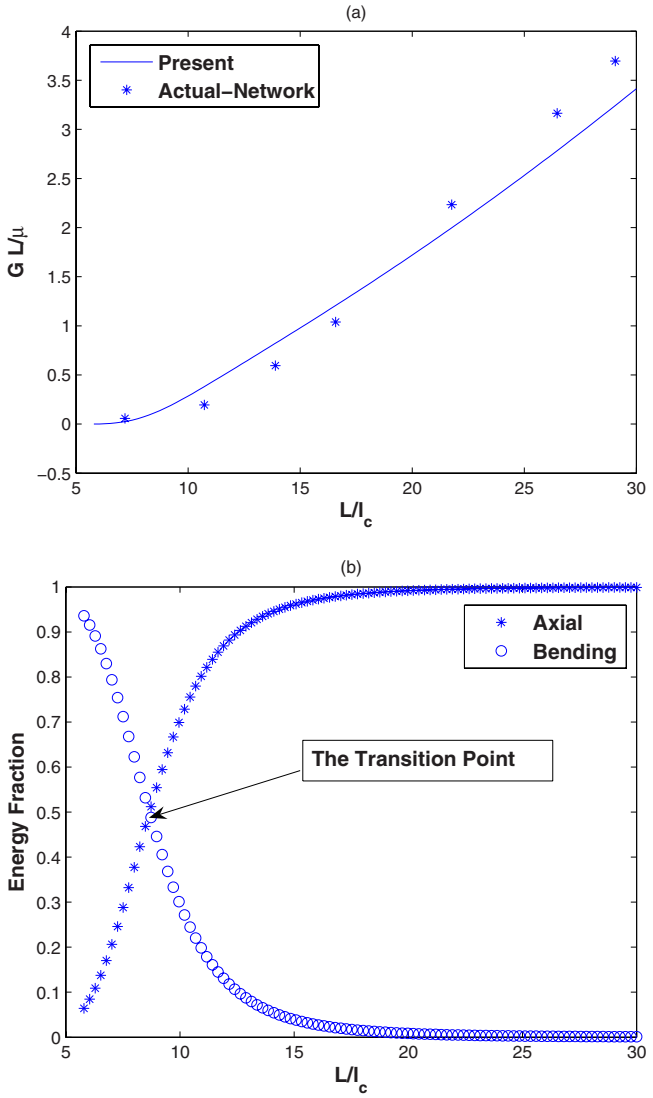

FIG. 7. (Color online) (a) Nondimensional shear modulus vs L/l_c and for $l_b/L=0.006$; (b) relative energy fraction for the same case.

$$\frac{U_{\text{axial}}}{U} = 1 - \frac{2}{2 + 3\frac{l_b^2}{L^2}\alpha^4(\alpha - 2)}. \tag{19}$$

Figure 6(b) shows the plot of the axial energy fraction vs l_b/L for the case of $L/l_c=29.09$. The axial energy fraction matches that obtained by Head *et al.* [13]. In Fig. 6(b), the linear portion of the curve signifies the nonaffine deformation regime. In the linear portion, the elastic modulus G is proportional to the bending rigidity κ and the elastic energy is mostly stored in the bending mode. An approximate equation for the linear portion of the curve in Fig. 6(b) can be obtained from Eq. (19) as

$$\frac{U_{\text{axial}}}{U} \approx \frac{3}{2}\frac{l_b^2}{L^2}\alpha^4(\alpha - 2). \tag{20}$$

Equation (20) is valid for

$$\frac{l_b}{L} \ll \frac{1}{\alpha^{5/2}}. \tag{21}$$

Substituting $\alpha=29.09$ we get $l_b/L \sim O(10^{-4})$. It is also seen that there is a cutoff l_b/L, above which the network attains its affine deformation mode, i.e., the whole network deforms in axial mode. As l_b/L increases, the bending modulus κ of the constituent fibers also increases; as a result, bending becomes increasingly less favorable deformation mode and the network preferentially deforms in axial mode. The macroscopic shear modulus asymptotically approaches its affine limit and the deformation energy is entirely stored as axial energy. Even without the spring, qualitatively we obtained similar behaviors (not shown) as those in Fig. 6. The gradual transition from the bending-dominated deformation to axial stretching can be attributed to the free rotations of the main chains about the joints and their continuous preferential topological adjustments to accommodate the axial deformation mode.

In Fig. 7(b), we plot the relative energy fractions for changing L/l_c and fixed $l_b/L=0.006$. It is observed that the bending energy fraction vanishes very fast with increasing cross-linking density, and for $L/l_c > 25$ the network deforms almost completely in the affine mode. As expected, the figure also validates that near the rigidity percolation threshold, $L/l_c|_{\text{crit}}=5.932$, the shear modulus is contributed predominantly by the bending deformation mode, and the modulus would have vanished if the fibers did not have any bending rigidity, i.e., $\kappa=0$ [30]. This is in agreement with what is observed from Mikado model simulations [9,14]. Near the rigidity percolation threshold, the axial energy fraction is less than 4%, which justifies the assumption of neglecting the finite-size effect of the network [14].

In the actual network as L/l_c increases, the cross-link sites become closer to each other and the bending deformation mode becomes increasingly energetically unfavorable; the network thus deforms in axial mode at a high cross-link density. In the unit cell model, this phenomenon is captured in the following way. As L/l_c increases, l_c becomes smaller and as a consequence the mid-square 5-6-7-8 tends to collapse to a point at the center of the unit cell and the main chains preferentially deform in axial mode.

Figure 8 shows a family of plots for the nondimensional shear modulus GL/μ vs L/l_c for different values of l_b/L. It is observed that as l_b/L increases (the bending rigidity κ of the individual fibers increases) the shear modulus asymptotically approaches the affine limit. The transition from the nonaffine to the affine regime takes place at a lower value of l_b/L with increasing network density L/l_c. The power law nature of the curves in Figs. 7(a) and 8 arises due to the percolating nature of the actual semiflexible network, which is captured in the model by the power law correction given in Eq. (15). At high L/l_c the asymptotic nature can be attributed to the increased geometrical constraints arising on the bending deformation due to progressively smaller l_c and a gradual transition from preferentially bending to preferentially axial deformation mode.

As discussed by Head *et al.* [9,10,13], there exists a length scale λ defined as

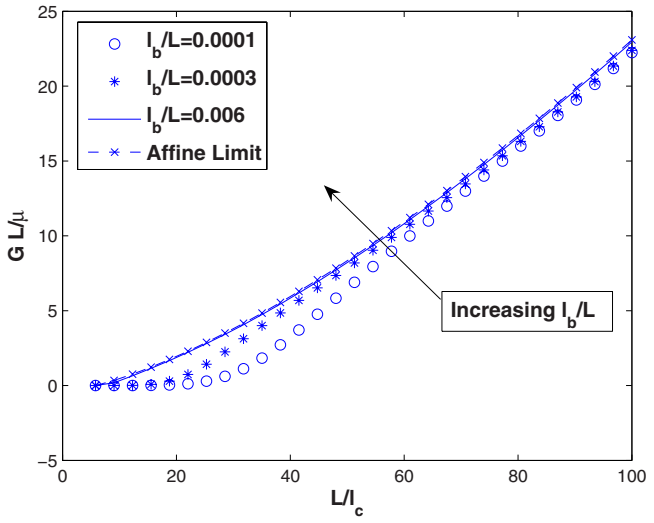

FIG. 8. (Color online) Normalized shear modulus vs L/l_c, for three different values of l_b/L.

$$\lambda = l_c\left(\frac{l_c}{l_b}\right)^z, \tag{22}$$

such that when G/G_{affine} is plotted vs L/λ all the curves collapse onto a master curve. This master curve can further be used to ascertain the affine and nonaffine regimes of deformation. In the unit cell model, we are also able to collapse G/G_{affine} curves onto a master curve, as shown in Fig. 9, with the exponent as $z=0.5882$ as compared to $z=0.4$ found by Head *et al.* [9,10,13]. The difference in the magnitude of the exponent is due to its model-dependent nature. As seen in Fig. 9, the ratio L/λ can be used to ascertain which regime the network is in, in the sense that $\lambda < L$ corresponds to the affine and $\lambda > L$ to the nonaffine regime.

C. The entropic effect on the modulus

Until now we have completely neglected the entropic effect on the network modulus. At finite temperature ($T>0$),

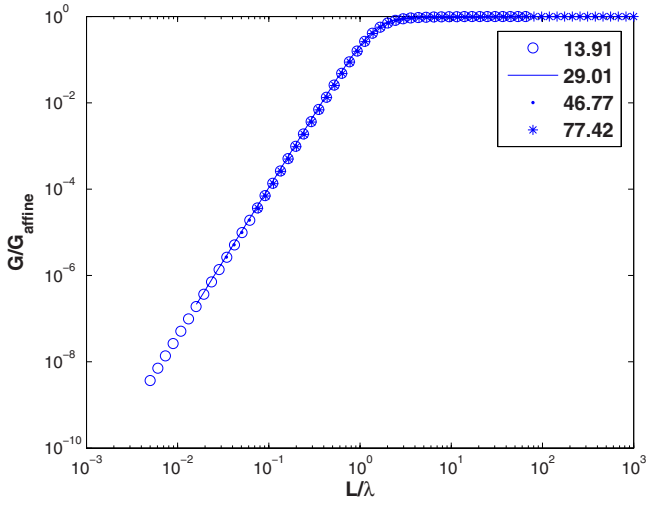

FIG. 9. (Color online) Collapse of the curves. With $z=0.5882$ in Eq. (18), all the curves collapse onto one master curve.

there will be transverse thermal fluctuations of the semiflexible fibers and estimation of the network modulus would require the inclusion of polymer configuration (waviness) as additional degrees of freedom [11]. Investigations on the single-molecular level revealed that the entropic effect will give rise to an additional longitudinal compliance [5] for the individual constituents. Physically, this compliance comes from the ability to pull out the thermal fluctuations of the filament, without stretching the filament backbone [5,9,13]. The entropic longitudinal modulus for a single semiflexible polymer chain of length L is given by [5]

$$\mu_T = \frac{90\kappa l_p}{L^3}, \tag{23}$$

where $l_p=\kappa/KT$ is the persistence length. The prefactor 90 reflects the local hinge boundary conditions. This entropic stiffness is thought to act in series with the enthalpic stiffness [10,13], and the resultant effective stiffness is given by

$$\frac{L}{\mu} = \frac{L}{\mu_T} + \frac{L}{\mu_M} \quad \text{or} \quad \mu = \frac{\mu_T\mu_M}{\mu_T+\mu_M}. \tag{24}$$

In Eq. (23), the bending stiffness $\kappa \sim Er^4$, and the axial enthalpic stiffness $\mu_M \sim Er^2$, where E is the Young's modulus and r is the radius of the individual fibers, respectively. Equation (23) gives

$$\mu_T \sim \frac{\kappa l_p}{L^3} \sim \frac{Er^4 l_p}{L^3} \sim \frac{r^2 l_p}{L^3}\mu_M. \tag{25}$$

Then the ratio $\aleph$ is defined as

$$\aleph = \frac{1/\mu_M}{1/\mu_T} \sim \frac{r^2 l_p}{L^3}. \tag{26}$$

From Eq. (26), if $\aleph \gg 1$ or $L \ll (r^2 l_p)^{1/3}$, the mechanical extensional compliance $1/\mu_M$ dominates. Therefore, over a length segment much smaller than $(r^2 l_p)^{1/3}$, the segment behaves like a straight rigid rod and for all practical purposes we can assume $\mu \approx \mu_M$. On the other hand, if $\aleph \ll 1$ or $L \gg (r^2 l_p)^{1/3}$, i.e., the thermal compliance $1/\mu_T$ dominates, for length segments much greater than $(r^2 l_p)^{1/3}$ we can assume $\mu \approx \mu_T$. For intermediate values of length segments we can use the stiffness given by Eq. (24) as mentioned by Head *et al.* [13]. Incorporation of the entropic effect in the above mentioned way gives a first approximation of the entropic effect to the actual network elasticity; for detailed analysis we need to incorporate the filament undulation between the cross-link points [31].

IV. CONCLUSION

This paper developed an efficient micromechanical model to predict the behavior of a cytoskeleton network over the whole parameter space. The model successfully captures the underlying deformation physics of the cytoskeleton network revealed from previous studies using computational models, such as the Mikado network model. Specifically, the proposed micromechanical model correctly captures the transition between the nonaffine and affine deformations, charac-

terized as the vanishing of the bending contribution to the overall deformation. Also, the present model is capable of giving an effective elastic modulus for a wide range of geometric and material parameter variations. In addition, a generalized length scale λ associated with the proposed micromechanical model has been identified, which signifies the cutoff between the affine and nonaffine deformation patterns. An advantage of the proposed model is that it provides an efficient way to determine the deformation energy of the cytoskeleton network, which previously could only be determined through costly computations of random network models. Since a continuum constitutive model requires a description of deformation energy under arbitrary deformation, the proposed model therefore provides an efficient way to develop a continuum constitutive model for the cytoskeleton, which is currently under study by the authors. After a continuum level constitutive model is developed, the mechanics of cytoskeletons with different shapes and nontrivial geometry and boundary conditions, such as those experienced by cells, can be considered by using the finite-element method integrated with the cytoskeleton constitutive model. The present work is based on observations from previous studies on a Mikado-type model, which captures some of the most essential physics of the cytoskeleton network. The model has not considered other effects, such as boundary effects and prestress, which are also important in cell mechanics. Also, the whole-cell behavior is complicated by chemomechanical coupling, structural adaptation, etc. This model is therefore a first step toward capturing the "live" properties of the whole cell. The authors are currently working on extending the present model to capture the effect of biochemical changes on the changing cross-linking density through a simple kinetic law, which will connect the L/l_c variable with the chemical energy input. The chemomechanical model will help in understanding some fundamental physics in cells.

ACKNOWLEDGMENT

The authors gratefully acknowledge financial support by NSF (Grant No. CMMI-0528548).

APPENDIX

For moderately large cross-link density, i.e., $\alpha=L/l_c \approx L_f/l_c$, the axial and bending spring constants are approximated as

$$k_a = \frac{2}{3}\frac{\mu}{L_f}\frac{\alpha(\alpha+1)(2\alpha+1)-1}{(\alpha+2)^2} \approx \frac{4}{3}\frac{\mu}{L}\alpha,$$

$$k_b = 3\frac{\kappa}{L_f^3}\frac{\alpha^6}{\alpha-1} \approx 3\frac{\kappa}{L^3}\alpha^5. \tag{A1}$$

Using the above approximations, the expression for G is given by

$$G \approx 6\mu L C^* \left(\frac{\alpha^2(2\alpha^5-10\alpha^4+14\alpha^3+16\alpha^2-64\alpha+64)\bar{l}_b^2+3\alpha^6(\alpha^6-7\alpha^5+17\alpha^4+18\alpha^3-168\alpha^2+280\alpha-104)\bar{l}_b^4+36\alpha^{10}(2\alpha^4-13\alpha^3+29\alpha^2-19\alpha-6)\bar{l}_b^6}{4(\alpha-2)^2+12\alpha(\alpha-2)^2(\alpha^4-2\alpha^3+16\alpha-12)\bar{l}_b^2+9\alpha^5(\alpha-2)^2(\alpha^5-4\alpha^4+4\alpha^3+48\alpha^2-112\alpha+32)\bar{l}_b^4+108\alpha^9(\alpha-2)^4(1+2\alpha)\bar{l}_b^6} \right), \tag{A2}$$

where $C^*=0.035(\alpha-5.932)^{1.4}/A_{\mathrm{uc}}$. Substituting $\bar{l}_b=l_b/L=\sqrt{\kappa/\mu}(1/L)$ in Eq. (A2) and taking the limit $\kappa\to\infty$, we can get the expression of G_{affine} as given in Eq. (17). By a simple order estimation, it can be shown that, in the linear portion of the curve in Fig. 6(a), $G/G_{\mathrm{affine}} \sim \alpha^5\bar{l}_b^2$, which on a log-log scale takes the form

$$\log\left(\frac{G}{G_{\mathrm{affine}}}\right) = 2\log(\bar{l}_b) + C. \tag{A3}$$

Using the moderately large cross-link density assumption as given in Eq. (A1), we can derive an expression for the energy fraction of the system as

$$\frac{U_a}{U} = 1 - \frac{2}{2+3\bar{l}_b^2\alpha^4(\alpha-2)} - \frac{4+3\bar{l}_b^2(\alpha^5-2\alpha^4+32\alpha^2-24\alpha)}{2+3\bar{l}_b^2(\alpha^5-2\alpha^4+32\alpha^2-24\alpha)+36\bar{l}_b^4(2\alpha^7-3\alpha^6-2\alpha^5)} + T_1, \tag{A4}$$

where T_1 is given by

$$T_1 = \frac{(4\alpha^5-20\alpha^4+28\alpha^3+32\alpha^2-128\alpha+128)+3\bar{l}_b^2\alpha^4(\alpha^6-7\alpha^5+17\alpha^4+18\alpha^3-168\alpha^2+280\alpha-104)}{(2\alpha^5-10\alpha^4+14\alpha^3+16\alpha^2-64\alpha+64)+3\bar{l}_b^2\alpha^4(\alpha^6-7\alpha^5+17\alpha^4+18\alpha^3-168\alpha^2+280\alpha-104)+36\bar{l}_b^4\alpha^8(2\alpha^4-13\alpha^3+29\alpha^2-19\alpha-6)}. \tag{A5}$$

Neglecting terms of $O(1/\alpha)$ relative to the terms of order 1, we can further simplify the third term and T_1 in Eq. (13). The simplified expressions are given as

$$\frac{4+3\bar{l}_b^2(\alpha^5-2\alpha^4+32\alpha^2-24\alpha)}{2+3\bar{l}_b^2(\alpha^5-2\alpha^4+32\alpha^2-24\alpha)+36\bar{l}_b^4(2\alpha^7-3\alpha^6-2\alpha^5)} \approx \frac{1}{1+24\alpha^2\bar{l}_b^2}, \tag{A6}$$

$$T_1 \approx \frac{1}{1+24\alpha^2\bar{l}_b^2}. \tag{A7}$$

It is seen that the third term and T_1 cancel each other out in the moderately large α limit. Equation (A4) can be simplified to the expression given in Eq. (19).

[1] *Cytoskeleton Mechanics, Models, and Measurements*, edited by R. K. M. Mohammad and R. D. Kamm (Cambridge University Press, Cambridge, U.K., 2006).
[2] B. Alberts *et al.*, *Molecular Biology of Cells*, 4th ed. (Garland Science, New York, 1994).
[3] P. A. Janmey *et al.*, J. Biol. Chem. **269**, 32503 (1994).
[4] J. Kas *et al.*, Biophys. J. **70**, 609 (1996).
[5] F. C. Mackintosh, J. Kas, and P. A. Janmey, Phys. Rev. Lett. **75**, 4425 (1995).
[6] M. Tempel, G. Isenberg, and E. Sackmann, Phys. Rev. E **54**, 1802 (1996).
[7] C. Storm *et al.*, Nature (London) **435**, 191 (2005).
[8] M. Rubinstein and R. H. Colby, *Polymer Physics* (Oxford University Press, Oxford, 2003).
[9] D. A. Head, A. J. Levine, and F. C. MacKintosh, Phys. Rev. Lett. **91**, 108102 (2003).
[10] D. A. Head, A. J. Levine, and F. C. MacKintosh, Phys. Rev. E **72**, 061914 (2005).
[11] J. Wilhelm and E. Frey, Phys. Rev. Lett. **91**, 108103 (2003).
[12] L. R. G. Treloar, *The Physics of Rubber Elasticity*, 2nd ed. (Clarendon Press, Oxford, 1958).
[13] D. A. Head, A. J. Levine, and F. C. MacKintosh, Phys. Rev. E **68**, 061907 (2003).
[14] D. A. Head, F. C. MacKintosh, and A. J. Levine, Phys. Rev. E **68**, 025101 (2003).
[15] A. Vaziri and A. Gopinath, Nat. Mater. **7**, 15 (2008).
[16] M. L. Gardel *et al.*, Science **304**(5675), 1301 (2004).
[17] M. Das, F. C. MacKintosh, and A. J. Levine, Phys. Rev. Lett. **99**, 038101 (2007).
[18] G. A. Holzapfel, *Nonlinear Solid Mechanics: A Continuum Approach for Engineering* (Wiley, Chichester, U.K., 2000).
[19] M. C. Boyce and E. M. Arruda, Rubber Chem. Technol. **73**, 504 (2000).
[20] S. C. Liu, L. H. Derick, and J. Palek, J. Cell Biol. **104**, 527 (1987).
[21] M. Arslan and M. C. Boyce, J. Appl. Mech. **73**, 536 (2006).
[22] X. F. Wu and Y. A. Dzenis, J. Appl. Phys. **98**, 093501 (2005).
[23] E. M. Arruda and M. C. Boyce, J. Mech. Phys. Solids **41**, 389 (1993).
[24] M. Sahimi, Lect. Notes Math. **1035**, 314 (1983).
[25] S. Arbabi and M. Sahimi, Phys. Rev. B **38**, 7173 (1988).
[26] S. Arbabi and M. Sahimi, J. Phys. A **21**, L863 (1988).
[27] S. Arbabi and M. Sahimi, Phys. Rev. Lett. **65**, 725 (1990).
[28] D. Stauffer and A. Aharony, *Introduction to Percolation Theory*, 2nd ed. (Taylor & Francis, London, 1992), p. 181.
[29] M. Latva-Kokko, J. Makinen, and J. Timonen, Phys. Rev. E **63**, 046113 (2001).
[30] M. Kellomaki, J. Astrom, and J. Timonen, Phys. Rev. Lett. **77**, 2730 (1996).
[31] E. M. Huisman *et al.*, Phys. Rev. Lett. **99**, 208103 (2007).
[32] E. Frey, ChemPhysChem **3**, 270 (2002).